Available online at www.sciencedirect.com
SCIENCE DIRECT®
Phytomedicine 13 (2006) 401–411
Phytomedicine
www.elsevier.de/phymed

Screening of novel nuclear receptor agonists by a convenient reporter gene assay system using green fluorescent protein derivatives

T. Suzuki[a,b], T. Nishimaki-Mogami[a], H. Kawai[a], T. Kobayashi[a], Y. Shinozaki[a], Y. Sato[a], T. Hashimoto[c], Y. Asakawa[c], K. Inoue[a], Y. Ohno[a], T. Hayakawa[a], T. Kawanishi[a,*]

[a]*National Institute of Health Sciences, Tokyo, Japan*
[b]*Pharmaceuticals and Medical Device Agency, Tokyo, Japan*
[c]*Faculty of Pharmaceutical Sciences, Tokushima Bunri University, Tokushima, Japan*

Received 27 September 2004; accepted 6 April 2005

Abstract

Nuclear receptors represent a very good family of protein targets for the prevention and treatment of diverse diseases. In this study, we screened natural compounds and their derivatives, and discovered ligands for the retinoic acid receptors (RARs) and the farnesoid X receptor (FXR). In the reporter assay systems of nuclear receptors presented here, two fluorescent proteins, enhanced yellow fluorescent protein (EYFP) and enhanced cyan fluorescent protein (ECFP), were used for detection of a ligand-based induction and as an internal control, respectively. By optimizing the conditions (e.g., of hormone response elements and promoter genes for reporter plasmids), we established a battery of assay systems for ligands of RARs, retinoid X receptor (RXR) and FXR. The screening using the reporter assay system can be carried out without the addition of co-factors or substrates. As a result of screening of more than 140 compounds, several compounds were detected which activate RARs and/or FXR. Caffeic acid phenylethyl ester (CAPE), known as a component of propolis from honeybee hives, and other derivatives of caffeic acid up-regulated the expression of reporter gene for RARs. Grifolin and ginkgolic acids, which are non-steroidal skeleton compounds purified from mushroom or ginkgo leaves, up-regulated the expression of the reporter gene for FXR.

Keywords: FXR; RAR; Reporter assay; Fluorescence; GFP; Caffeic acid; Ginkgolic acid; Grifolin

Introduction

Nuclear hormone receptors are ligand-activated transcription factors that are involved in a variety of physiological, developmental, and toxicological processes. The nuclear hormone receptor superfamily includes receptors for thyroid and steroid hormones, retinoids and vitamin D, as well as receptors for unknown ligands. These receptors share a highly conserved DNA-binding domain and a discrete ligand-binding domain, and bind to hormone response elements (HREs) on the DNA during the formation of homodimers, heterodimers, or monomers. This ligand binding to nuclear receptors leads to conformational

*Corresponding author. Tel.: +81 3 3700 9064; fax: +81 3 3700 9084.
E-mail address: kawanish@nihs.go.jp (T. Kawanishi).

0944-7113/$ - see front matter © 2005 Elsevier GmbH. All rights reserved.
doi:10.1016/j.phymed.2005.09.003

change of these receptors and the recruitment of coactivator complexes, resulting in transcriptional activation (Khorasanizadeh and Rastinejad, 2001). Their ligand-dependent activity makes nuclear receptors good pharmacological targets.

Nuclear receptors form a superfamily of phylogenetically related proteins encoded by 48 genes in the human genome. Three isotypes of retinoic acid receptors (RARs: RARα, RARβ and RARγ) are receptors for retinoids such as all-*trans*-retinoic acid (ATRA) (Petkovich et al., 1987; Brand et al., 1988; Krust et al., 1989). RARα is associated with differentiation therapy for human acute promyelocytic leukemia (Hansen et al., 2000). RARβ plays a central role in limiting the growth of different cell types (reviewed in Hansen et al., 2000), and is thus a possible target for the treatment of breast and other cancers. RARγ is also primarily expressed in the skin and is involved in skin photoaging and carcinogenesis, and in skin diseases such as psoriasis and acne (Fisher et al., 1996).

The farnesoid X receptor (FXR) is a receptor for bile acids such as chenodeoxycholic acid (CDCA), deoxycholic acid, cholic acid, and their conjugates. Bile acids are synthesized in the liver and secreted into the intestine, where their physical properties facilitate the absorption of fats and vitamins through micelle formation. Cholesterol disposal from the liver is also dependent on the bile acid composition of the secreted bile. Bile acids bind to FXR to activate and regulate the transcription of FXR target genes. FXR controls the expression of critical genes in bile acid and cholesterol homeostasis (Makishima et al., 1999; Parks et al., 1999; Wang et al., 1999). FXR-null mice show elevated serum cholesterol and triglyceride levels (Sinal et al., 2000), and an FXR agonist has been shown to reduce serum triglyceride levels (Maloney et al., 2000). FXR is thus an attractive pharmacological target for the treatment of hyperlipidemia. Moreover, an FXR agonist has been reported to confer hepatoprotection in a rat model of cholestasis (Liu et al., 2003).

The retinoid X receptor (RXR) is a common heterodimeric partner for many receptors, including thyroid hormone receptor (TR), RAR, vitamin D_3 receptor (VDR), peroxisome proliferator-activated receptor (PPAR), liver X receptor (LXR), and FXR, in addition to functioning as a receptor for 9-*cis*-retinoic acid (9CRA) during formation of a homodimer.

To determine ligands for these nuclear receptors, we developed a reporter assay system using GFP derivatives. To study the promoter and enhancer control of gene expression, firefly luciferase is widely used as a reporter protein because it has high sensitivity and a broad linear range. In the commonly used reporter assay, β-galactosidase, a well-characterized bacterial enzyme, or renilla luciferase is usually used in conjunction with firefly luciferase to normalize the transfection efficiency of the reporter gene (Sherf et al., 1996; Martin et al., 1996). In such cases, the activity of the two reporter proteins must be measured in different ways (e.g., absorptiometry and luminescence photometry) or by using two substrates. In the reporter assay presented here, we used two species derived from green fluorescent protein (GFP), one (enhanced yellow fluorescent protein, (EYFP)) to measure the promotion and enhancement of gene expression, and the other (enhanced cyan fluorescent protein, (ECFP)) to normalize the transfection, and were thus able to measure the fluorescent protein signals simultaneously without any co-factor or substrates. As a result of screening of more than 140 compounds, it was found that several compounds activate RARs and/or FXR.

Materials and methods

Chemicals

Chenodeoxycholic acid was purchased from Sigma-Aldrich (St. Louis, MI, USA), and ATRA and 9CRA were from Wako (Osaka, Japan). Ginkgolic acid 17:1, 15:0, and 13:0 were purchased from Nagara Science (Gifu, Japan).

Purification and synthesis of test compounds

Ginkgolic acid 15:1 was purified from *Ginkgo biloba L.* var. *diptera* according to Morimoto et al. (1968). 2-Methyl ginkgolic acid methyl ester was prepared by methylation of the ginkgolic acid with methyl iodide and K_2CO_3 (Paul and Yeddanapalli, 1956; Begum et al., 2002). Grifolin was purified from *Albatrellus confluens* and *Albatrellus ovinus* (Ishii et al., 1988; Nukata et al., 2002). We isolated bazzanenyl caffeate from the liverwort *Bazzania fauriana* (Toyota and Asakawa, 1988). We synthesized caffeic acid phenethyl ester (CAPE), farnesyl caffeate and geranyl caffeate for acquirement in quantity. The synthesis of CAPE by coupling reactions of caffeic acid and β-phenylethyl bromide was reported by Hashimoto et al. (1988), and the details of the synthesis of farnesyl and geranyl caffeates are described below. The purity of the compounds for the bioactivation test was shown to be over 95% by ^1H and ^{13}C NMR spectra.

Synthesis of farnesyl caffeate

Twenty-five percent NaOH (2.5 ml) was added to a solution of caffeic acid (3,4-dihydroxycinnamic acid) (2.10 g) in HMPA (hexamethylphosphoric triamide) (150 ml), and the mixture was stirred for 1 h under N_2 at room temperature. A solution of farnesyl bromide (4.98 g) in HMPA (20 ml) was added dropwise for

10 min to the reaction mixture. The reaction mixture was stirred for 24 h at room temperature, and poured in ice cold H_2O (300 ml). The organic layer, which was extracted with Et_2O (200 ml × 2), was washed with brine (300 ml), dried ($MgSO_4$) and evaporated under reduced pressure to an oil (6.75 g). The oil was chromatographed on silica gel (200 g) with a gradient solvent system of $CHCl_3$–EtOAc, increasing the amount of 2% portions EtOAc stepwise to give 32 fractions. Farnesyl caffeate (1.435 g; Y. 43.2%) was obtained from 10% EtOAc-*n*-hexane eluate (Fr. 12-18) as a pure white powder. Caffeic acid (1.025 g; Y. 48.8%), the starting material, was recovered from 20% EtOAc-*n*-hexane eluate (Fr. 25-31).

Farnesyl caffeate: EI-MS: *m/z* 384 (M^+,5%), 315, 204, 180, 163 (100%), 135, 93, 69; HR-MS: *m/z* 384.2307, $C_{24}H_{32}O_4$ requires 384.2300; anal. calcd. for $C_{24}H_{32}O_4$: C, 74.97; H, 8.39. Found: C, 74.85; H, 8.30; FT-IR (KBr) cm^{-1}: 3480 (OH), 3301 (OH), 1678 (C=O), 1600, 1278, 1183; UV (EtOH) λ_{max} nm (log ε): 333 (4.15), 303 (4.00), 248 (3.90), 220 (4.03); ^{1}H NMR (acetone-d_6): δ1.56 (3H, *s*, CH_3), 1.62 (3H, *s*, CH_3), 1.65 (3H, *s*, CH_3), 1.76 (3H, *s*, CH_3), 4.68 (1H, *d*, *J* = 7.0 Hz, H-1′), 5.12 (2H, *m*, H-6′ and H-10′), 5.41 (1H, *t*, *J* = 7.0 Hz, H-2′), 6.26 (1H, *d*, *J* = 15.9 Hz, H-β), 6.87 (1H, *d*, *J* = 8.2 Hz, H-5), 7.03 (1H, *dd*, *J* = 1.8, 8.2 Hz, H-6), 7.15 (1H, *d*, *J* = 1.8 Hz, H-2), 7.53 (1H, *d*, *J* = 15.9 Hz, H-α), 8.26 (1H, *br.s*, –OH), 8.49 (1H, *br.s*, –OH); ^{13}C NMR ((acetone-d_6): δ16.1 (*q*, CH_3), 16.4 (*q*, CH_3), 17.7 (*q*, CH_3), 25.8 (*q*, CH_3), 26.8 (*t*, CH_2), 27.4 (*t*, CH_2), 40.1 (*t*, CH_2), 40.4 (*t*, CH_2), 61.3 (*t*, CH_2), 115.1 (*d*, CH), 115.7 (*d*, CH), 116.3 (*d*, CH), 120.1 (*d*, CH), 122.4 (*d*, CH), 124.6 (*d*, CH), 125.1 (*d*, CH), 127.6 (*s*, C), 131.6 (*s*, C), 135.9 (*s*, C), 142.1 (*s*, C), 145.6 (*d*, CH), 146.3 (*s*, C), 148.7 (*s*, C), 167.3 (*s*, –COO)).

Synthesis of geranyl caffeate

Twenty-five percent NaOH (2.1 ml) was added to a solution of caffeic acid (2.00 g) in HMPA (150 ml), and the mixture was stirred for 1 h under N_2 at room temperature. A solution of geranyl bromide (3.10 g) in HMPA (20 ml) was added dropwise for 10 min to the reaction mixture. The reaction mixture was treated further as described above to afford geranyl caffeate (1.48 g; Y. 61.4%) as a white powder, and caffeic acid (0.56 g; Y. 28.0%).

Geranyl caffeate: EI-MS: *m/z* 316 (M^+, 10%), 247, 180, 163 (100%), 136, 69; HR-MS: *m/z* 316.1682, $C_{19}H_{24}O_4$ requires 316.1674; anal. calcd. for $C_{19}H_{24}O_4$: C, 72.12; H, 7.65. Found: C, 72.01; H, 7.68; FT-IR (KBr) cm^{-1}: 3483 (OH), 3295 (OH), 1678 (C=O), 1599, 1278, 1183; UV (EtOH) λ_{max} nm (log ε): 334 (4.16), 302 (4.05), 249 (3.93), 222 (4.01); ^{1}H NMR (acetone-d_6): δ1.60 (3H, *s*, CH_3), 1.66 (3H, *s*, CH_3), 1.75 (3H, *s*, CH_3), 4.68 (1H, *d*, *J* = 7.0 Hz, H-1′), 5.12 (1H, *t*, *J* = 7.0 Hz, H-6′), 5.40 (1H, *t*, *J* = 7.0 Hz, H-2′), 6.27 (1H, *d*, *J* = 15.9 Hz, H-β), 6.87 (1H, *d*, *J* = 8.2 Hz, H-5), 7.03 (1H, *dd*, *J* = 2.0, 8.2 Hz, H-6), 7.16 (1H, *d*, *J* = 2.0 Hz, H-2), 7.55 (1H, *d*, *J* = 15.9 Hz, H-α), 8.28 (1H, *br.s*, –OH), 8.50 (1H, *br.s*, –OH); ^{13}C NMR ((acetone-d_6): δ16.4 (*q*, CH_3), 17.7(*q*, CH_3), 25.8 (*q*, CH_3), 27.0 (*t*, CH_2), 40.1 (*t*, CH_2), 61.3 (*t*, CH_2), 115.1 (*d*, CH), 115.6 (*d*, CH), 116.3 (*d*, CH), 120.0 (*d*, CH), 122.4 (*d*, CH), 124.6 (*d*, CH), 127.6 (*s*, C), 132.0 (*s*, C), 142.1 (*s*, C), 145.6 (*d*, CH), 146.3 (*s*, C), 148.7 (*s*, C), 167.3 (*s*, –COO)).

Plasmid construction

Plasmids were constructed for the expression of RXRα, FXR and RARs. The ORF regions of human RXRα, human FXR, mouse RARα1, mouse RARβ2, and mouse RARγ1 (accession numbers X52773, U68233, X57528, S56660, X15848) were amplified by PCR and inserted into pcDNA3.1 (Invitrogen, Carlsbad, CA, USA), respectively. For reporter plasmids, the luciferase region of the pGL3-Control Vector (Promega, Madison, WI, USA) was replaced with the EYFP fragment of pEYFP-N1 or the ECFP fragment of pECFP-N1 (Clontech, Palo Alto, CA, USA) using *Nco*I and *Xba*I sites. Subsequently, the simian virus 40 (SV40) early promoter was cut out with *Bgl*II and *Hin*dIII, and replaced with the thymidine kinase (TK) promoter of the pRL-TK vector (Promega) or one of several other promoters (the 3′ region of the TK promoter, the cytomegalovirus (CMV) promoter, or the minimal CMV promoter and the 3′ region of the CMV promoter (201 and 265 bp)) amplified using the following PCR primers:

5′-ggagatctggccccgcccagcgtcttgtc-3′ and 5′-ggaagcttgcggcacgctgttgacgctgttaagcgggtcgctgcaggg-3′ (3′ region of the TK promoter);
5′-ccagatcttagttattaatagtaatcaattacggggtc-3′ and 5′-ccaagcttgatctgacggttcactaaaccagc-3′ (CMV promoter);
5′-ccagatcttaggcgtgtacggtgggagg-3′ and 5′-ccaagcttaggctggatcggtcccggtg-3′ (minimal CMV promoter);
5′-ccagatcttgggagtttgttttggcacc-3′ and reverse primer of CMV promoter (CMV 201); and
5′-ccagatcttcaatgggcgtggatagcgg-3′ and reverse primer of CMV promoter (CMV265).

Double-stranded oligonucleotides containing HREs (RXRE, RARE and FXRE; shown in Fig. 1B) were ligated into the upstream region of these promoters using *Mlu*I and *Bgl*II sites. The sequences of the constructed plasmids were confirmed by sequencing using an ABI PRISM 310 Genetic Analyzer (Applied Biosystems, Foster City, CA, USA).

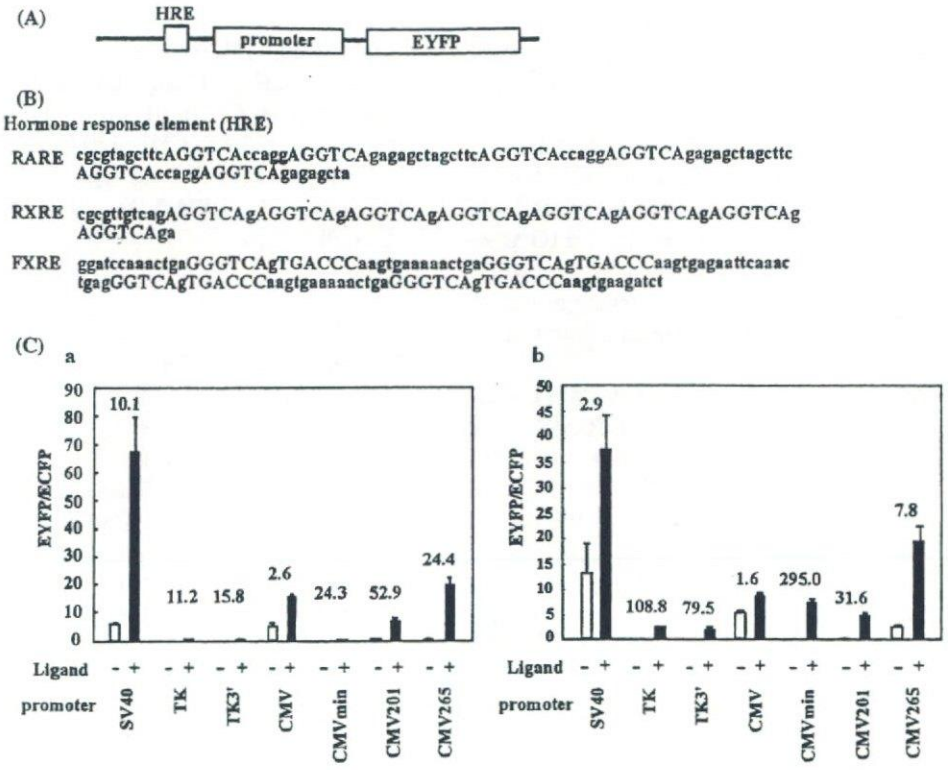

Fig. 1. Reporter plasmids for the assay of nuclear receptors. (A) Model of the constructed reporter plasmids. (B) The sequences for HREs of RAR, RXR and FXR (RARE, RXRE, and FXRE). (C) Effect of different promoters on the reporter assay. Seven species of promoter were employed in the reporter plasmid containing the HRE and EYFP genes. The activations of RARα (a) and FXR (b) are shown. The transfected cells were treated with ligands (black bar), 1 μM of ATRA for the RAR reporter assay or 100 μM of CDCA for FXR, or DMSO as a vehicle (white bar). The vertical axis indicates the ratio of fluorescence of EYFP (signal) to ECFP (internal control). The fold response relative to vehicle-treated cells is shown above the bars. Data are shown as the means + SD derived from six experiments.

Cotransfection and reporter assay

A monkey kidney cell line, COS-7, was kept in DMEM with 10% FBS. Transfections were performed using an Effectene transfection reagent (Qiagen, Valencia, CA) according to the manufacturer's instructions. The ratio of the reporter plasmid, receptor expression plasmids (for example, the RARα and RXRα expression plasmids for assay of RARα ligands) and the internal control plasmid was 4:1:1:1. The culture medium was replaced with DMEM without phenol red (Gibco BRL, Gaithersburg, MD) supplemented with 10% charcoal-treated FBS (Hyclone, Logan, UT) when the transfections were performed. At 15 h after transfections, the cells were treated with trypsin/penicillin reagent and divided among wells of a black, 96-well plate with 100 μl of the culture medium. At 6 h after division among wells, the cells were treated with chemicals. After a 40-h incubation, the medium was eliminated by decantation, the cells were washed twice with PBS, and the wells were filled with 200 μl PBS. Fluorescence was detected using a microplate reader (ARVO; Perkin Elmer, Fremont, CA, USA). The fluorescence of EYFP was detected with an excitation filter of 485 nm and an emission filter of 545 nm, and that of ECFP was detected with filters of 420 and 486 nm (Perkin Elmer), respectively. The autofluorescence in COS-7 cells was subtracted from each of the detected fluorescences, and the EYFP/ECFP ratio was calculated using the resulting values.

Results

Reporter assay system

In the present reporter assay, EYFP and ECFP were selected as a reporter protein and an internal control for normalization of transfection, respectively. These two fluorescent proteins were chosen, because the peaks of their excitation and emission wavelengths are sufficiently different (a difference of 80 and 50 nm,

respectively) so that they can be detected simultaneously without cross-detection. The considerable cross-detection between EYFP and ECFP could be prevented using a set of optical filters (see Materials and methods). The EYFP/ECFP ratio was calculated after the autofluorescence of COS-7 cells was subtracted from the fluorescence intensities of EYFP and ECFP, because the autofluorescence was not negligible.

The reporter plasmids were constructed as shown in Fig. 1A. As HREs for FXR (FXR-RXR heterodimer), RAR (RAR-RXR heterodimer) and RXR (RXR homodimer), the fragments shown in Fig. 1B were used. In order to amplify signals, we employed three copies of DR5 (direct repeat with 5 bp of spacing) and four copies of DR1 as RAR and RXR response elements (RARE and RXRE). For the FXR response element (FXRE), four copies of the response element (inverted repeat) existing in the upstream region of the phospholipid transfer protein (PLTP) gene were employed. The tandem repeats in HREs elevated the response to a sufficient degree to detect the chemicals that activated the receptor. Then, an appropriate promoter for enhancing the fluorescent signal while retaining the response to the chemicals was selected from among seven promoters (Fig. 1C). Since the SV40 or CMV promoter caused a high fluorescence intensity with or without ligands, the responses to the ligands were not strong. The response of the RAR reporter plasmid with the SV40 promoter was about ten-fold. However, the apparent rate of the response was enhanced by interference of the expression of ECFP by the expression of EYFP, because the same promoter was employed for the reporter plasmid and the internal control plasmid. Therefore, the rate did not reflect a real response, and had a large SD. The TK promoter, the 3′ region of the TK promoter and the minimal CMV promoter caused strong responses, but the expression in the control plasmid was too low for quantitative measurement. The expression of reporter proteins with the 3′ region of the CMV promoter was higher than that with TK or the minimal CMV promoter, maintaining the induction rate by the ligands. Based on a comparison between the 3′ regions of the CMV promoters, we selected the CMV201 (201 bp of the CMV promoter) promoter for use in the experiments below, since the response of CMV201 was stronger than that of CMV265.

In addition to the promoter for reporter plasmids, the promoter for the internal control plasmid and the expression plasmids of nuclear receptors were examined in order to establish an appropriate assay system of the nuclear receptor ligands. When the SV40 promoter was employed for the expression of ECFP in the internal control plasmid, the SV40 promoter for nuclear receptor expression interfered with the expression of ECFP (data not shown). Therefore, the CMV promoter was employed for nuclear receptor expression plasmids. Finally, we established the following plasmid set as the reporter assay system: a reporter plasmid containing the EYFP gene, whose expression was regulated by the HRE and CMV201 promoter; an internal control plasmid containing the ECFP gene expressed by the SV40 promoter; and the expression plasmid of the nuclear receptor containing each nuclear receptor gene expressed by the CMV promoter.

Fig. 2A shows the response to typical agonists for FXR, RARs and RXRα in the screening system. For screening of RAR ligands, three subtypes of RARs (RARα1, RARβ2, RARγ1) were expressed in the cells independently. Although endogenous RARs co-exists in the cell, the preference for the subtype of compounds could be detected. Fig. 2B and C show the dose-dependence of the assay system of FXR and RAR ligands, respectively. RARs were activated by 100 pM of ATRA. ED_{50} values were estimated to be about 1–10 nM for RARα and 0.1–1 nM for RARβ and RARγ (only the result of RARα is shown in Fig. 2B). On the other hand, activation of FXR was seen in 3–10 μM CDCA and greater activation was observed at 100 μM CDCA (Fig. 2C). These dose-dependent response patterns were comparable to those reported previously (Brand et al., 1988; Parks et al., 1999), indicating that these assays could be used for quantitative measurement of the activation by ligands. The established method of the reporter assay was described in Materials and methods.

Screening of a novel ligand for nuclear receptors

Using the established screening system, we found some natural compounds and their derivatives which acted as agonists for RARs and FXR. In the screening, there was a possibility that unexpected factors may have changed the signal responses (in the present assay system, the transcriptional efficiency may be changed irrespective of the nuclear receptor, the tested chemicals may have their own fluorescence, and so forth). Therefore, another reporter plasmid without HRE was also constructed to eliminate these unexpected factors. As this plasmid was used in place of the reporter plasmid, the compounds that regulated the expression of EYFP without HRE were eliminated. Some results of the response for each nuclear receptor are shown in Fig. 3 (RAR, upper panel; FXR, middle panel; control, lower panel). The results for RARβ are presented as representative of those for RARs. Ten millimolar of each compound referring to the stock solution in DMSO was added to the culture medium of the transfected COS-7 cells at a final concentration of 30 μM (Fig. 3, Nos. 1–26). Compound Nos. 27, 28, and 29 were 3 μM ATRA, 30 μM CDCA, and vehicle, respectively. ATRA also slightly activated the FXR-RXR heterodimer, due

to the activation of RXR. Although, for example, Nos. 16, 18, 19, and 25 enhanced the relative EYFP/ECFP ratio, these compounds also enhanced the control that was used with the reporter plasmid without HRE. Thus it was concluded that these compounds were not ligands for the nuclear receptors.

As a result of screening more than 140 compounds (a part of the results is shown in Fig. 3), five compounds were found as ligands for the nuclear receptors. CAPE (compound No. 20 in Fig. 3), geranyl caffeate (No. 21), and farnesyl caffeate (not shown in Fig. 3) were found to be RAR agonists. Ginkgolic acid 15:1 (No. 12), geranyl caffeate (No. 21), and grifolin (No. 26) were found to be FXR agonists.

The structures of the caffeic acid derivatives tested in the screening are shown in Fig. 4A. CAPE, known as an active compound of propolis from honeybee hives, was synthesized from caffeic acid and β-phenylethyl bromide and other caffeic acids were purified and synthesized as described in Materials and methods. Three of these compounds (i.e., all of those tested except for bazzanenyl caffeate) activated RARs (Fig. 4B). The cells treated with over 30 μM of these compounds were removed from wells by washing of the reporter assay, because these compounds were toxic to the cell. Therefore, the results shown are for a reporter assay conducted using lower concentrations. Although the activation of RARs could be hardly detected by a low concentration of caffeic acid-derivatives, the activation by the compounds 10–30 μM was comparable to maximum activation by ATRA. As shown in Fig. 4B, CAPE activated RARβ to a greater degree than RARα or RARγ.

As FXR agonists, geranyl caffeate, ginkgolic acid 15:1 and grifolin were found. Geranyl caffeate, the RAR agonist, highly activated FXR (Fig. 3, No. 21), but the activation of the RXR homodimer was not detected (data not shown). It could not be determined whether or not farnesyl caffeate, a compound similar to geranyl caffeate, activated FXR, because 30 μM of these compounds showed toxicity for cells. The structures of ginkgolic acids and grifolin are shown in Fig. 5A. It has been reported that ginkgolic acid 15:1 was present in ginkgolic leaves (Ahlemeyer et al., 2001), and grifolin in mushrooms (Hirata and Nakanishi, 1949; Sugiyama et al., 1992). The activations of FXR by ginkgolic acid 15:1 and geranyl caffeate were comparable to that by CDCA,

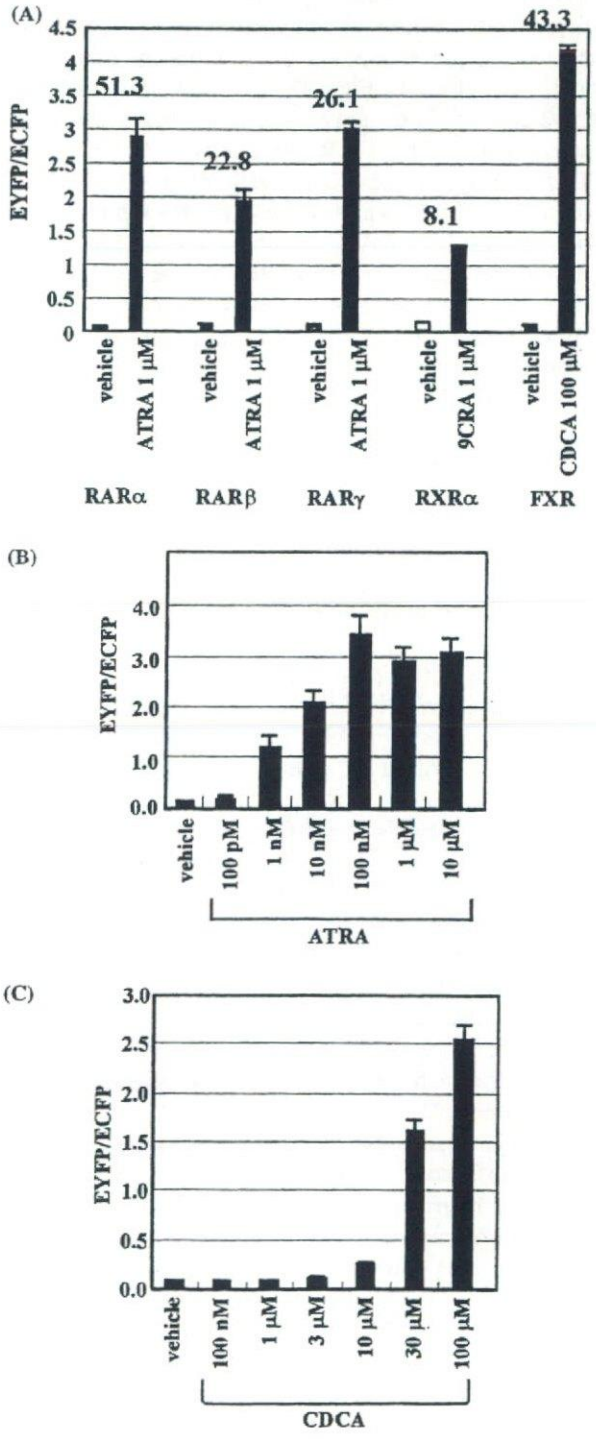

Fig. 2. Response in the reporter expression. (A) The responses in the reporter assay system by typical agonists for RAR, RXR, and FXR. COS-7 cells were transfected with an appropriate set of the plasmids (e.g. for assay of RARα ligand, the reporter plasmid containing RARE, the expression plasmids of RARα and RXRα and the internal control plasmid; for assay of RXRα ligand, the reporter plasmid containing RXRE, the RXRα expression plasmid, and the internal control plasmid). The transfected cells were treated with 1 μM of ATRA, 1 μM of 9CRA, or 100 μM of CDCA as ligands (black bar), or DMSO as a vehicle (white bar). The response rate is shown above the bars. Data are shown as the means + SD derived from three experiments. (B), (C) Dose–response analyses of ATRA and CDCA on the reporter assay of RAR and FXR. Data are shown as the means + SD derived from four experiments.

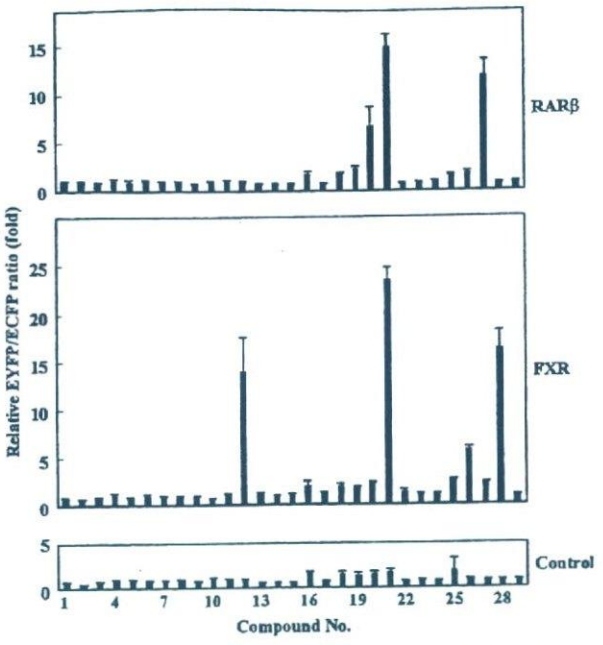

Fig. 3. Screening of ligands for RAR and FXR. COS-7 cells were transfected with the reporter plasmid, the receptor expression plasmid, and the internal control plasmid as shown in Fig. 2. The cells were treated with 30 μM of each compound. The results of the screening for RAR are shown in the upper panel, those for FXR in the middle panel, and those for the control (no HRE) in the lower panel. The results for RARβ are presented as representative of those for RARs (No. 1, hydrangeic acid; No. 2, ethyl 4′-ethylhydrangenate; No. 3, hydrangenol; No. 4, 8,3′-dimethoxyphylodulcin; No. 5, macrophyllaside A; No. 6, yashabashiletodiol A; No. 7, lycogarbin C; No. 8, lycogarbin A; No. 9, polygodial; No. 10, sacculatal; No. 11, ptychantin A; No. 12, ginkgolic acid 15:1; No. 13, 2-methyl ginkgolic acid methyl ester; No. 14, bilobal dimethyl ether; No. 15, 3-tridecanyl-*m*-cresol; No. 16, [11]-cytochalasa-6(12),13-diene-1,21-dione-7,18-dihydroxy-16,18-dimethyl-19-methoxy-10-phenyl-(7*S**,13*E*,16*S**,18*S**,19*R**); No. 17, hispidin; No. 18, costunolide, No. 19, beta-cyclocostanolide; No. 20, caffeic acid phenethyl ester; No. 21, geranyl caffeate; No. 22, atroctylon).

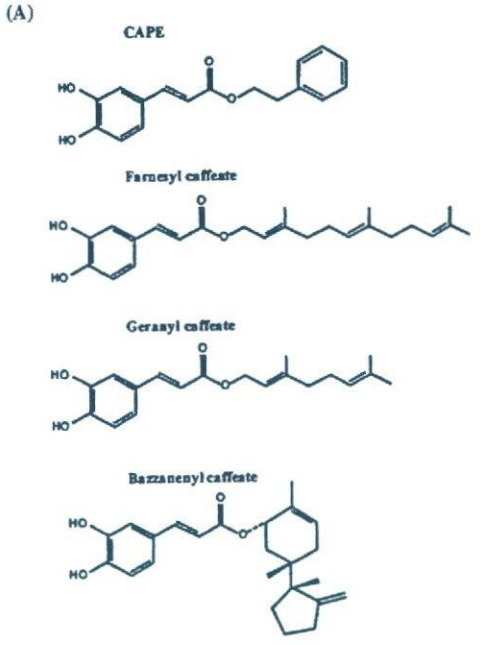

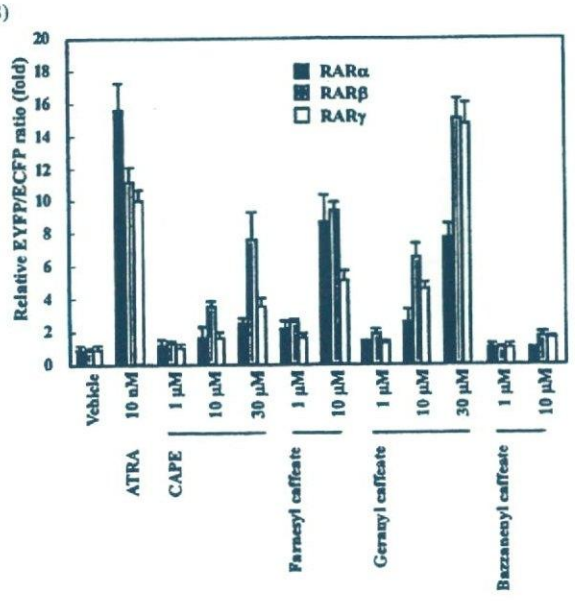

Fig. 4. Ligands for RARs. (A) The structures of caffeic acid derivatives tested in the screening. (B) Response in the RAR reporter assay. The responses in the COS-7 cells expressing RARα, RARβ or RARγ are indicated by black, gray, and white bars, respectively. Data are expressed as the fold response relative to vehicle (0.1% DMSO)-treated cells and are shown as the means + SD derived from four experiments.

the most potent endogenous bile acid. Ginkgolic acids 17:1, 15:0 and 13:0 (described in Fig. 5A) were also investigated as the other ginkgolic acids of ginkgo leaves (Fig. 5B). Ginkgolic acid 17:1 activated FXR more strongly than did 15:1, and ginkgolic acids with an alkyl chain (13:0, 15:0) activated FXR at concentrations of more than 20 μM. It seemed that the double bond and length of the carbon chain had an influence on FXR activation. Moreover, the structures except for the carbon chain were also important for FXR activation, because the methylated compound of ginkgolic acid 15:1 (2-methyl ginkgolic acid methyl ester, Fig. 5A) had no potency for FXR activation (Fig. 3, No. 13).

Discussion

To discover ligands for the nuclear receptors, we developed a battery of reporter assay systems

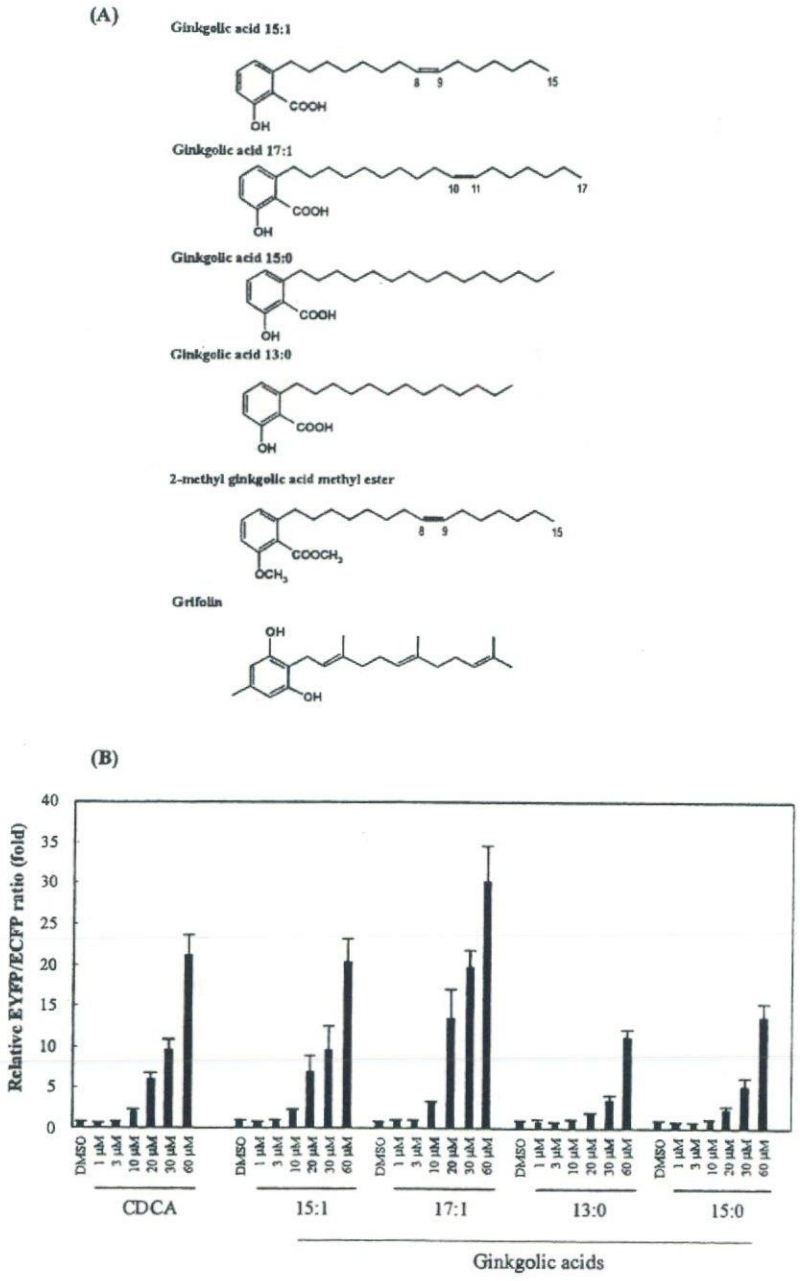

Fig. 5. Ligands for FXR. (A) The structure of candidates for FXR agonists and their related compounds (2-methyl ginkgolic acid methyl ester). (B) The activation of FXR by ginkgolic acids. COS-7 cells were transfected with the reporter plasmid containing FXRE, the expression plasmids of FXR and RXRα and the internal control plasmid. The transfected cells were treated with each compound. Data are shown as the means + SD derived from four experiments.

incorporating the advantages of fluorescent proteins. The disadvantage of GFP (low sensitivity) could be overcome by modifications. The present screening system using fluorescent proteins has clear merits of a high efficiency, convenience and low cost, because the two fluorescent signals can be measured simultaneously without addition of any co-factors. Moreover, the fluorescent signal was stable for more than 2 h after the wash. Considering these merits, this reporter assay system with fluorescent proteins might be advantageous for automatic high-throughput screening. If the expression of the fluorescent protein can be increased, the measurement of fluorescence can be carried out in culture medium, and the signal can be measured by time-course without any treatment. Moreover, the use of three fluorescent proteins (for example, DsRed with EYFP and ECFP) would enable us to carry out more efficient measurement.

Using this assay system, several compounds that induce expression of the reporter gene for RARs and/or FXR were identified. These compounds were described as ligands in this report, although there is a possibility that these compounds are metabolized and their metabolites bind to the receptors as ligands.

Three new ligands for RARs were identified: CAPE, geranyl caffeate, and farnesyl caffeate. The whole structure of these compounds may be needed for RAR-activation, because caffeic acid, a constituent compound of the compounds, did not activate RARs (data not shown). CAPE has been reported to have antioxidant, antiviral, anti-inflammatory and immunomodulatory activities (Grunberger et al., 1988), and has also been shown to inhibit the growth of different types of oncogene-transformed cells and to induce apoptosis (Grunberger et al., 1988; Burke et al., 1995; Su et al., 1994; Watabe et al., 2004). Since RARs have been reported to mediate many biological processes, it is possible that some of the diverse activities are due to their binding to RARs. Since geranyl and farnesyl caffeate have also been reported to exert antioxidant effects and to inhibit the growth of cancer cells (Inoue et al., 2004), the three compounds may suppress the growth of cancer by at least two pathways: induction of RAR and antioxidant effects. Considering its preferential activation of RARβ (Fig. 4B), CAPE may inhibit cancer (e.g., lung cancer) growth more selectively without substantial toxicity, such as the triglyceride elevation associated with RARα, and the skin, bone and teratogenic toxicity associated with RARγ Thus, especially CAPE could be assumed to be a seed for the development of an anti-cancer drug.

We also found that two natural compounds, ginkgolic acids and grifolin, activated FXR. Grifolin was first isolated as an antibiotic constituent of a mushroom, *Grifola confluens* (Hirata and Nakanishi, 1949). In 1992, it was reported that grifolin decreased liver cholesterol content, plasma total cholesterol levels, and plasma (very low-density lipoprotein (VLDL) + low-density lipoprotein (LDL)) cholesterol levels, and increased plasma high-density lipoprotein (HDL) cholesterol and plasma triglyceride levels (Sugiyama et al., 1992). It has been suggested that the effect of grifolin might be elicited, at least in part, by the augmented excretion of cholesterol into the faces (Sugiyama et al., 1994). On the other hand, FXR controls the expression of critical genes in bile acid and cholesterol homeostasis. In fact, FXR-null mice show elevated serum cholesterol and triglyceride levels (Sinal et al., 2000), and an FXR agonist has been shown to reduce serum triglyceride levels (Maloney et al., 2000). Moreover, FXR induces the expression of the gene of PLTP, which plays a role in HDL metabolism (Urizar et al., 2000). It seems that the cholesterol-lowering and HDL-cholesterol-increasing effects of grifolin are related to FXR activation, although grifolin's enhancement of triglyceride production was not consistent with its down-regulation of FXR agonists.

The FXR agonists found in this study are all non-steroidal compounds, whereas the well-known ligand of FXR, bile acid, is a steroidal one. The common characteristic of the structure of the ligands is their long carbon chains (i.e., geranyl, farnesyl and pentadecenyl), and farnesol has been shown to be a FXR ligand (Forman et al., 1995). However, aspects of the structures other than the carbon chains also appear to be important for FXR activation, because geraniol, a constituent compound of geranyl caffeate, has been reported not to activate FXR (Forman et al., 1995), and the methylated compound of ginkgolic acid 15:1 had no potency for FXR activation in the present study.

Several compounds, such as TTNPB, GW4064, Farnesoid, Forskolin, Fexaramine, AGN29 and AGN31, have been reported as non-steroidal agonists (Maloney et al., 2000; Howard et al., 2000; Downes et al., 2003; Dussault et al., 2003). The non-steroidal ligands may be important tools for studying the pharmacology of the receptor, because they may not have the property of bile acids and are not metabolized to form harmful lithocholic acid (Fischer et al., 1996; Javitt, 1966). In the present study, ginkgolic acids and geranyl caffeate strongly activated FXR, and both had structures quite different from bile acids, so that they could be good tools in this sense. Moreover, the importance of identifying gene-selective modulators that regulate a subset of FXR-specific genes as therapeutic agents has been recognized (Cui et al., 2003; Dussault et al., 2003). The gene-selective modulators of estrogen receptor, selective estrogen receptor modulators (SERMs), have been well studied (reviewed in McDonnell et al., 2002), and some compounds with a structure divergent from that of estrogen have been identified and applied to therapies of breast cancer and osteoporosis. The non-steroidal compounds could also be good tools for studying the selective response of FXR target genes.

In this report, we developed a new method for screening novel nuclear receptor agonists, and used it to identify new candidate ligands for FXR and RARs. We expect that these new ligands will be good pharmacological tools. Since the compound whose structure is much different from bile acids is expected to possess a specific effect as a ligand, we continue to screen various ligands from natural compounds with a wide variety of structures.

Acknowledgements

This work was supported by a grant-in-aid (MF-16) from the Pharmaceuticals and Medical Device Agency, a grant-in-aid for Research on Health Sciences Focusing

on Drug Innovation from the Japan Health Science Foundation, and a grant-in-aid for Research on Advanced Medical Technology from the Ministry of Health, Labour and Welfare of Japan.

References

Ahlemeyer, B., Selke, D., Schaper, C., Klumpp, S., Krieglstein, J., 2001. Ginkgolic acids induce neuronal death and activate protein phosphatase type-2C. Eur. J. Pharmacol. 430, 1–7.

Begum, P., Hashidoko, Y., Islam, M.T., Ogawa, Y., Tahara, S., 2002. Zoosporicidal activities of anacardic acids against *Aphanomyces cochlioides*. Z. Naturforsch. [C] 57, 874–882.

Brand, N., Petkovich, M., Krust, A., Chambon, P., de Thé, H., Marchio, A., Tiollais, P., Dejean, A., 1988. Identification of a second human retinoic acid receptor. Nature 332, 850–853.

Burke Jr., T.R., Fesen, M.R., Mazumder, A., Wang, J., Carothers, A.M., Grunberger, D., Driscoll, J., Kohn, K., Pommier, Y., 1995. Hydroxylated aromatic inhibitors of HIV-1 intergrase. J. Med. Chem. 38, 4171–4178.

Cui, J., Huang, L., Zhao, A., Lew, J.-L., Yu, J., Sahoo, S., Meinke, P.T., Royo, I., Peláez, F., Wright, S.D., 2003. Guggulsterone is a farnesoid X receptor antagonist in coactivator association assays but acts to enhance transcription of bile salt export pump. J. Biol. Chem. 278, 10214–10220.

Downes, M., Verdecia, M.A., Roecker, A.J., Hughes, R., Hogenesch, J.B., Kast-Woelbern, H.R., Bowman, M.E., Ferrer, J.-L., Anisfeld, A.M., Edwards, P.A., Rosenfeld, J.M., Alvarez, J.G.A., Noel, J.P., Nicolaou, K.C., Evans, R.M., 2003. A chemical, genetic, and structural analysis of the nuclear bile acid receptor FXR. Mol. Cell 11, 1079–1092.

Dussault, I., Beard, R., Lin, M., Hollister, K., Chen, J., Xiao, J.H., Chandraratna, R., Forman, B.M., 2003. Identification of gene-selective modulators of the bile acid receptor FXR. J. Biol. Chem. 278, 7027–7033.

Fischer, S., Beuers, U., Spengler, U., Zwiebel, F.M., Koebe, H.G., 1996. Hepatic levels of bile acids in end-stage chronic cholestatic liver disease. Clin. Chim. Acta 251, 173–186.

Fisher, G.J., Voorhees, J.J., 1996. Molecular mechanisms of retinoid actions in skin. FASEB J. 10, 1002–1013.

Forman, B.M., Goode, E., Chen, J., Oro, A.E., Bradley, D.J., Perlmann, T., Noonan, D.J., Burka, L.T., McMorris, T., Lamph, W.W., Evans, R.M., Weinberger, C., 1995. Identification of a nuclear receptor that is activated by farnesol metabolites. Cell 81, 687–693.

Grunberger, D., Banerjee, R., Eisinger, K., Oltz, E.M., Efros, L., Caldwell, M., Estevez, V., Nakanishi, K., 1988. Preferential cytotoxity on tumor cells by caffeic acid phenethyl ester isolated from propolis. Experientia 44, 230–232.

Hansen, L.A., Sigman, C.C., Andreola, F., Ross, S.A., Kelloff, G.J., De Luca, L.M., 2000. Retinoids in chemoprevention and differentiation therapy. Carcinogenesis 21, 1271–1279.

Hashimoto, T., Tori, M., Asakawa, Y., Wollenweber, E., 1988. Synthesis of two allergenic constituents of propolis and poplar bud excretion. Z. Naturforsch. [C] 43, 470–472.

Hirata, Y., Nakanishi, K., 1949. Grifolin, an antibiotic from a basidiomycete. J. Biol. Chem. 184, 135–143.

Howard, W.R., Pospisil, J.A., Njolito, E., Noonan, D.J., 2000. Catabolites of cholesterol synthesis pathways and forskolin as activators of the farnesoid X-activated nuclear receptor. Toxicol. Appl. Pharmacol. 163, 195–202.

Inoue, K., Nishitani, N., Tanabe, A., Yamanaka, H., Hashimoto, T., Asakawa, Y., Fujiki, H., 2004. Significance of structural specificity in the antioxidant activity of hydrangenol and caffeic acid-derivatives. Abstract for 124th Congress on Nihon yakugakukai, Osaka, Japan, vol. 2, p. 173.

Ishii, N., Takahashi, A., Kusano, G., Nozoe, S., 1988. Studies on the constituents of *Polyporus dispansus* and *P. confluens*. Chem. Pharm. Bull. 36, 2918–2924.

Javitt, N.B., 1966. Cholestasis in rats induced by taurolithocholate. Nature 210, 1262–1263.

Khorasanizadeh, S., Rastinejad, F., 2001. Nuclear–receptor interactions on DNA-response elements. Trends Biochem. Sci. 26, 384–390.

Krust, A., Kastner, P.H., Petkovich, M., Zelent, A., Chambon, P., 1989. A third human retinoic acid receptor, hRAR-γ. Proc. Natl. Acad. Sci. USA 86, 5310–5314.

Liu, Y., Binz, J., Numerick, M.J., Dennis, S., Luo, G., Desai, B., MacKenzie, K.I., Mansfield, T.A., Kliewer, S.A., Goodwin, B., Jones, S.A., 2003. Hepatoprotection by the farnesoid X receptor agonist GW4064 in rat models of intra- and extrahepatic cholestasis. J. Clin. Invest. 112, 1678–1687.

Makishima, M., Okamoto, A.Y., Repa, J.J., Tu, H., Learned, R.M., Luk, A., Hull, M.V., Lustig, K.D., Mangelsdorf, D.J., Shan, B., 1999. Identification of a nuclear receptor for bile acids. Science 284, 1362–1365.

Maloney, P.R., Parks, D.J., Haffner, C.D., Fivush, A.M., Chandra, G., Plunket, K.D., Creech, K.L., Moore, L.B., Wilson, J.G., Lewis, M.C., Jones, S.A., Willson, T.M., 2000. Identification of a chemical tool for the orphan nuclear receptor FXR. J. Med. Chem. 43, 2971–2974.

Martin, C.S., Wight, P.A., Dobretsova, A., Bronstein, I., 1996. Dual luminescence-based reporter gene assay for luciferase and β-galactosidase. Biotechniques 21, 520–524.

McDonnell, D.P., Connor, C.E., Wijayaratne, A., Chang, C.Y., Norris, J.D., 2002. Definition of the molecular and cellular mechanisms underlying the tissue-selective agonist/antagonist activities of selective estrogen receptor modulators. Recent Prog. Horm. Res. 57, 295–316.

Morimoto, H., Kawamatsu, Y., Sugihara, H., 1968. Stereostructure of toxin from the fruit of *Ginkgo biloba L.* Chem. Pharm. Bull. 16, 2282–2286.

Nukata, M., Hashimoto, T., Yamamoto, I., Iwasaki, N., Tanaka, M., Asakawa, Y., 2002. Neogrifolin derivatives possessing anti-oxidative activity from the mushroom *Albatrellus ovinus*. Phytochemistry 59, 731–737.

Parks, D.J., Blanchard, S.G., Bledsoe, R.K., Chandra, G., Consler, T.G., Kliewer, S.A., Stimmel, J.B., Willson, T.M., Zavacki, A.M., Moore, D.D., Lehmann, J.M., 1999. Bile acids: natural ligands for an orphan nuclear receptor. Science 284, 1365–1368.

Paul, V.J., Yeddanapalli, L.M., 1956. On the olefinic nature of anacardic acid from Indian cashew nut shell liquid. J. Am. Chem. Soc. 78, 5675–5678.

Petkovich, M., Brand, N.J., Krust, A., Chambon, P., 1987. A human retinoic acid receptor which belongs to the family of nuclear receptors. Nature 330, 444–450.

Sherf, B.A., Navarro, S.L., Hannah, R.R., Wood, K.V., 1996. Dual-luciferase™ reporter assay: an advanced co-reporter technology integrating firefly and *Renilla* luciferase assays. Promega Notes 57, 2.

Sinal, C.J., Tohkin, M., Miyata, M., Ward, J.M., Lambert, G., Gonzalez, F.J., 2000. Targeted disruption of the nuclear receptor FXR/BAR impairs bile acid and lipid homeostasis. Cell 102, 731–744.

Su, Z.-Z., Lin, J., Grunberger, D., Fisher, P.B., 1994. Growth suppression and toxicity induced by caffeic acid phenethyl ester (CAPE) in type 5 adenovirus-transformed rat embryo cells correlate directly with transformation progression. Cancer Res. 54, 1865–1870.

Sugiyama, K., Kawagishi, H., Tanaka, A., Saeki, S., Yoshida, S., Sakamoto, H., Ishiguro, Y., 1992. Isolation of plasma cholesterol-lowering components from Ningyotake (*Polyporus confluens*) mushroom. J. Nutr. Sci. Vitaminol. 38, 335–342.

Sugiyama, K., Tanaka, A., Kawagishi, H., Ojima, F., Sakamoto, H., Ishiguro, Y., 1994. Hypocholesterolemic action of dietary grifolin on rats fed with a high-cholesterol diet. Biosci. Biotechnol. Biochem. 58, 211–212.

Toyota, M., Asakawa, Y., 1988. Sesquiterpenoids from the liverwort *Bazzania fauriana*. Phytochemistry 27, 2155–2159.

Urizar, N.L., Dowhan, D.H., Moore, D.D., 2000. The farnesoid X-activated receptor mediates bile acid activation of phospholipid transfer protein gene expression. J. Biol. Chem. 275, 39313–39317.

Wang, H., Chen, J., Hollister, K., Sowers, L.C., Forman, B.M., 1999. Endogenous bile acids are ligands for the nuclear receptor FXR/BAR. Mol. Cell 3, 543–553.

Watabe, M., Hishikawa, K., Takayanagi, A., Shimizu, N., Nakaki, T., 2004. Caffeic acid phenethyl ester induces apoptosis by inhibition of NFκB and activation of Fas in human breast cancer MCF-7 cells. J. Biol. Chem. 279, 6017–6026.

J Pharmacol Sci 103, 159 – 167 (2007)

Journal of Pharmacological Sciences

Full Paper

Caspase Cascade Proceeds Rapidly After Cytochrome *c* Release From Mitochondria in Tumor Necrosis Factor-α-Induced Cell Death

Hiroshi Kawai[1,3,*], Takuo Suzuki[1], Tetsu Kobayashi[1], Akiko Ishii-Watabe[1], Haruna Sakurai[2], Hisayuki Ohata[2], Kazuo Honda[2], Kazutaka Momose[2], Takao Hayakawa[1], and Toru Kawanishi[1,#]

[1]*Division of Biological Chemistry and Biologicals, National Institute of Health Sciences, Tokyo 158-8501, Japan*
[2]*Department of Pharmacology, School of Pharmaceutical Sciences, Showa University, Tokyo 142-8555, Japan*
[3]*Faculty of Pharmaceutical Sciences, Josai International University, Chiba 283-8555, Japan*

Received August 2, 2006; Accepted December 2, 2006

Abstract. The caspase activation cascade and mitochondrial changes are major biochemical reactions in the apoptotic cell death machinery. We attempted to clarify the temporal relationship between caspase activation, cytochrome *c* release, mitochondrial depolarization, and morphological changes that take place during tumor necrosis factor (TNF)-α-induced cell death in HeLa cells. These reactions were analyzed at the single-cell level with 0.5 – 1 min resolution by using green fluorescent protein (GFP)-variant-derived probes and chemical probes. Cytochrome *c* release, caspase activation, and cellular shrinkage were always observed in this order within 10 min in all dying cells. This sequence of events was thus considered a critical pathway of cell death. Mitochondrial depolarization was also observed in all dying cells observed, but frequently occurred after caspase activation and cellular shrinkage. Mitochondrial depolarization is therefore likely to be a reaction that does not induce caspase activation and subsequent cellular shrinkage. Mitochondrial changes are important for apoptotic cell death; moreover, cytochrome *c* release, and not depolarization, is a key reaction related to cell death. In addition, we also found that the apoptotic pathway proceeds only when cells are exposed to TNF-α. These findings suggest that the entire cell death process proceeds rapidly during TNF-α exposure.

Keywords: tumor necrosis factor (TNF)-α, cytochrome *c*, mitochondrial depolarization, caspase, real-time imaging

Introduction

Apoptosis is a mechanism of cell death that is mediated by various intracellular reactions. A family of cysteine proteases, the caspases, forms the activation cascade, and these proteases play a central role in the apoptotic cell death machinery (1, 2). The caspases usually exist as pro-proteins in living cells and are activated by cleavage at the time when cell death is induced. In an early phase of the cell death process, initiator caspases are activated, which in turn activate effector caspases (3 – 7). Activated effector caspases cleave a number of different target proteins, and this cleavage leads ultimately to apoptotic cell death (8, 9). Mitochondria also play an important role in the cell death process (10 – 13). Cellular stresses induce mitochondrial changes, including an increase in outer mitochondrial membrane permeability; various mitochondrial proteins such as cytochrome *c* (cyt.*c*) and second mitochondrial activator of caspases (Smac) are released into the cytosol. Released proteins directly or indirectly regulate caspase activation and/or other reactions, which eventually induce cell death.

Various factors in the cell death process have been identified, but correlation among these factors remains unclear. Cell death events such as caspase activation and mitochondrial changes are rapid processes, and the onset of these events varies between individual cells (14 – 17). So, it is difficult to determine how and when such

*Corresponding author (affiliation #3). hkawai@jiu.ac.jp
#Present affiliation: Division of Drugs, National Institute of Health Sciences, Tokyo 158-8501, Japan
Published online in J-STAGE: February 8, 2007
doi: 10.1254/jphs.FP0060877

reactions occur in cells as based on analyses of cell populations, which can only be used to detect an average value for a large number of individual cells. In order to gain a better understanding of the cell death mechanism, simultaneous multi-events analyses should be conducted at the single-cell level and with high spatial and temporal resolution. Real-time imaging with confocal microscopy is a powerful method of detecting the manner in which such rapid intracellular reactions take place (18, 19).

Fluorescence resonance energy transfer (FRET) is useful for imaging analyses. Variants of green fluorescent protein (GFP) are currently widely employed; several families of fluorescent proteins have recently been reported to be useful for FRET analysis (19 – 22). Previously, we developed genetically-encoded sensors for caspase activation that consist of two fluorescent proteins linked by a small peptide (23, 24). Cyan-, green-, yellow-, and red-fluorescent proteins (CFP, GFP, YFP, DsRed) were used in combination as the fluorescent proteins. The small peptide was derived from a substrate of caspase, poly(ADP-ribose)polymerase; this fusion protein was primarily cleaved by caspase 3 (23). The sensor protein exhibits FRET in its intact form. However, in the presence of active caspase, the peptide is cleaved, and the two fluorescent proteins are rendered far apart; in this case, the sensor protein no longer exhibits any FRET. Caspase activation is detected as a reduction in FRET. We have previously reported that the use of various color combinations facilitates real-time imaging analysis. In particular, GFP-DsRed and YFP-DsRed have been shown to be as sensitive as CFP-YFP, which is commonly used as the FRET pair. FRET probes that consist of such color variations may be useful for simultaneous multi-event imaging (24).

In this study, we used the YFP-DsRed version of the effector-caspase sensor (YRec), CFP-tagged cyt.*c* (cyt.*c*-CFP), and tetramethylrhodamine methyl ester (TMRM) in order to detect caspase activation, cyt.*c* release from the mitochondria, and mitochondrial depolarization, respectively. By applying two of these probes simultaneously, two events could be monitored in the same cell, and the temporal relationships between caspase activation and mitochondrial changes could be examined at the single-cell level. In addition, we also analyzed the interval from tumor necrosis factor (TNF)-α exposure to cellular shrinkage by analyzing the cell population in order to investigate time course of the whole cell death process.

Materials and Methods

Plasmid construction

A plasmid encoding YRec, YFP-peptide-DsRed, was generated as previously reported (24). The sequence encoding the 11 amino acids at the C-terminus of YFP was eliminated in this construct. The C-terminal-truncated forms of the YFP gene were generated by PCR with primers containing the NheI site or the BspEI site and pEYFP-C1 (Clontech, Palo Alto, CA, USA) as a template, and the restricted fragment was inserted into the NheI/BspEI sites of pEYFP-C1 in order to generate a plasmid carrying truncated YFP. The oligonucleotides encoding the caspase's substrate sequence was inserted into the BspEI – AgeI site of the p(truncated YFP)-C1 vector to generate pYFP-PARP. The substrate sequence was derived from PARP (KRKGDEVDGVDE, 5'-CCGGAAAGAGAAAAGG CGATGAGGTGGATGGAGTGGATGAA-3' and 5'-CCGGTTCATCCACTCCATCCACCTCATCGCCTTT TCTCTTT-3'). DsRed was generated from pDsRed2-C1(Clontech) by PCR, at the AgeI/NotI sites, and the restricted fragment was inserted into the AgeI – NotI sites of pYFP-PARP to generate a plasmid carrying YFP-PARP-DsRed2 (YRec). YRec was cleaved by caspase-3 (23, 24).

Cyt.*c* was cloned from HeLa cells by RT-PCR with a primer pair (5'-TCGCTAGCGCTCCGGAGAATTAAA TATGGGTATG-3' and 5'-CGAGGATCCCTCATTAG TAGCTTTTTTGAG-3'), and the restricted fragment was inserted into the NheI – BamHI sites of the pECFP-N1 vector to generate a plasmid carrying cyt.*c*-CFP. All cloned sequences were verified by sequencing.

Cell culture and transfection

HeLa cells were cultured in DMEM (Sigma-Aldrich, St. Louis, MO, USA) supplemented with 100 units/ml of penicillin G, 100 μg/ml of streptomycin, and 10% fetal calf serum (GIBCO). The plasmid encoding the fluorescent probes was transfected into HeLa cells using Effectene Transfection Reagent (QIAGEN, Hilden, Germany) according to the manufacturer's instructions. After being incubated for 12 – 24 h with the transfection reagent, the cells were washed with PBS and cultivated on dishes suitable for an assay in medium containing 500 μg/ml of G418 for an additional 1 – 3 days until the assay was performed. We found that the cultivation period had no effect on cell death events after TNF-α treatment.

Bioimaging with fluorescence microscopy

Transfected cells were cultured on a cover glass (25-mm diameter, 0.15 – 0.18-mm thickness) for 1 – 3 days. Cells were treated with TNF-α (100 ng/ml, dissolved in PBS) and cycloheximide (10 μg/ml, dissolved in DMSO) and then were incubated under the usual culture conditions for 1 – 2 h prior to the analysis.

Table 1. Measurement conditions for real-time analysis by LSM510

Probe	Excitation (nm)	Beam splitter (nm)	Emission (nm)
Cyt.*c*-CFP	458	515	467.5 – 497.5
YRec	488	545	505 – 530 (donor)[a]
			560 – 615 (acceptor)[a]
TMRM	543	545	560 –[b]

[a]Emitted fluorescence was separated by a 545 dichroic mirror, and the fluorescence of the donor (YFP) and that of the acceptor (DsRed) was obtained via a band-pass emission filter. [b]A long-pass filter (LP560) was used.

Tetramethylrhodamine methyl ester (TMRM; 50 nM, dissolved in DMSO) was added to each sample 20 – 30 min prior to the analysis, when the mitochondrial membrane potential was to be measured (23, 25). Analyses were carried out by confocal laser scanning fluorescent microscopy using a Carl Zeiss LSM510 system (Carl Zeiss, Jena, Germany). During the observations, the media were buffered with 10 mM HEPES buffer (pH 7.4), and the cells were maintained at 35°C – 37°C. DIC images and grayscale images for fluorescence channels were obtained in 0.5- or 1-min intervals. Excitation lights for the cyt.*c*-CFP (458 nm) and YRec (488 nm) were provided by an Ar laser with a 458 or a 488 dichroic mirror, respectively. Excitation lights for the TMRM (543 nm) were provided by a HeNe laser with a 543 dichroic mirror. Images of the probes were obtained separately using a dichroic mirror and band-pass or long-pass emission filters, as indicated in Table 1. Contamination of the fluorescence between channels was negligible under these conditions (data not shown). For analyses involving YRec or TMRM, images were processed and quantified using MetaFluor software as follows: The average pixel intensity of the fluorescence of the entire cell region was determined for each channel. In the case of YRec, the ratio value was calculated as the average pixel value of the fluorescence ratio, (fluorescent intensity for the acceptor channel) /(fluorescent intensity for the donor channel), in the entire cell region. As the cells changed morphologically during the observation, the entire cell region was assessed separately for each image.

Simultaneous measurement of two probes was performed according to the multi-track scanning mode, in which two sets of excitation-detection conditions were used in alternation. For cyt.*c*-CFP and YRec, CFP fluorescence induced by excitation at 458 nm was measured in the first track, and YFP and DsRed fluorescence induced by excitation at 488 nm was measured in the second track. For cyt.*c*-CFP and TMRM, CFP fluorescence induced by excitation at 458 nm was measured in the first track, and TMRM fluorescence induced by excitation at 543 nm was measured in the second track. The scanning time difference between tracks was ca. 3 – 8 s, which was not significant in the temporal analysis.

Analysis of cell survival rate

HeLa cells were cultured in 96-well plastic plates to 80% – 90% confluency and were then treated with TNF-α. After the indicated culture durations, the cells were treated with Alamar Blue (Dainippon Pharmaceutical, Osaka) according to the manufacturer's instructions. Cell survival was measured as fluorescence at 590 nm induced by excitation at 540 nm. Fluorescence was measured using FlexStation (Molecular Devices, Sunnyvale, CA, USA).

Results

Simultaneous imaging of cyt.c-CFP and caspase sensor

HeLa cells expressing both cyt.*c*-CFP and YRec were treated with TNF-α, and changes in fluorescence were observed. Figure 1A shows DIC images, fluorescent images of CFP, and fluorescence ratio (DsRed/YFP) images of YRec during cell death. Images were obtained every 30 s; therefore, we were able to identify the time points of these events at a resolution period of 30 s. The CFP fluorescence indicated cyt.*c*-CFP localization, and the fluorescence ratio (DsRed/YFP) indicated caspase activation. CFP fluorescence was localized in the mitochondria at 280.5 min, and it was delocalized at 281.0 min, indicating that cyt.*c*-CFP was released during this period. The images shown in Fig. 1A indicate that this cell started to shrink at 286.5 – 287.0 min.

When the caspase was activated in a cell, the YRec was cleaved, which led to a reduction in the FRET from YFP to DsRed. Thus, a reduction in the fluorescence ratio (DsRed/YFP) reflected caspase activation. As shown in Fig. 1B, the fluorescence ratio decreased dramatically at 283.5 min in the cell shown here, thus indicating the initiation of caspase activation at this point in time. The increase in DsRed fluorescence

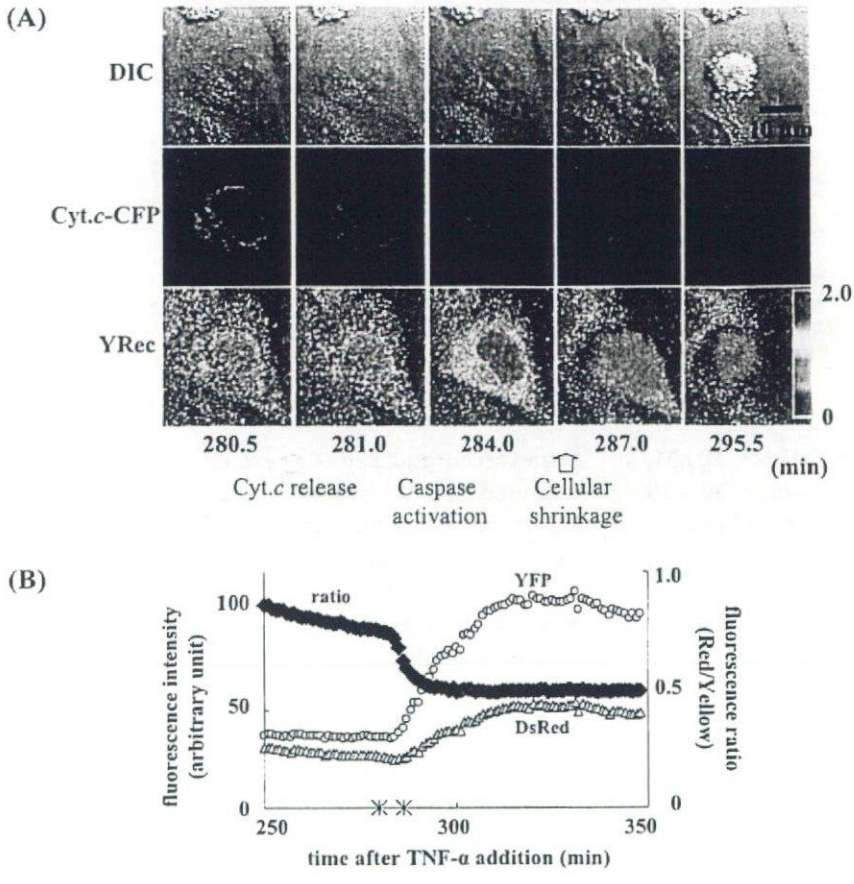

Fig. 1. Cyt.*c*-CFP release and caspase activation were monitored simultaneously in the same cells. A: DIC (upper), images showing the fluorescence of CFP (middle) and the fluorescence ratio of DsRed and YFP (DsRed /YFP, lower) during cell death are shown in pseudocolor. CFP and DsRed/YFP indicate the localization of cyt.*c*-CFP and caspase activation, respectively. B: Changes in YRec fluorescence in the cell shown in panel A were plotted. YFP and DsRed are shown with their fluorescence ratios. The asterisks indicate time points at which cyt.*c*-CFP were released and cell shrinkage was observed. The horizontal axis represents the point in time after the addition of TNF-*α*.

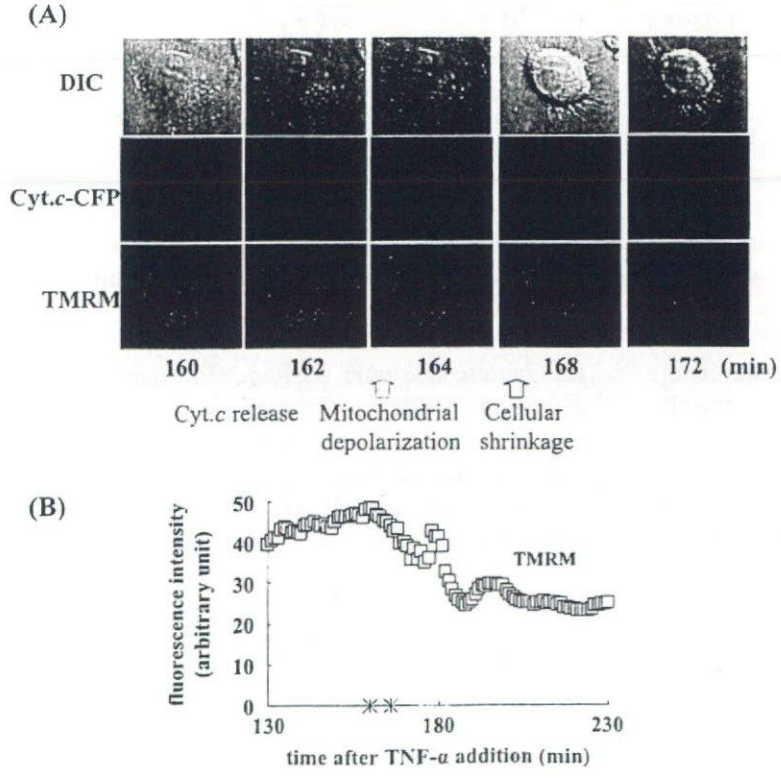

Fig. 2. Cyt.*c*-CFP release and mitochondrial depolarization were monitored simultaneously in the same cell. A: DIC (upper), images showing the fluorescence of CFP (middle) and the fluorescence of TMRM (lower) during cell death are shown in pseudocolor. CFP and TMRM fluorescence indicate the localization of cyt.*c*-CFP and the mitochondrial membrane potential, respectively. B: Changes in TMRM fluorescence of the cells in panel A during cell death were plotted. The asterisks indicate time points at which cyt.*c*-CFP were released and cell shrinkage was observed. The horizontal axis represents the point in time after the addition of TNF-*α*.

observed after this time point was unexpected, but is thought to have been the result of cellular shrinkage. Because the cell volume was reduced, the DsRed became concentrated, and the fluorescence increased. The reduction in the fluorescence ratio clearly indicated a reduction in FRET, which indicated both the cleavage of YRec as well as caspase activation. The asterisks indicate the time point of cyt.*c*-CFP release and cellular shrinkage, as determined based on the results shown in Fig. 1A. In this cell, cyt.*c*-CFP was released 280.5 min after the addition of TNF-α, and caspase activation was initiated 3 min after cyt.*c*-CFP release; the cell then started to shrink 3 min after caspase activation. Cyt.*c*-CFP release, caspase activation, and cellular shrinkage were observed in this order in all of the dying cells examined.

Simultaneous imaging of cyt.c-CFP and TMRM

HeLa cells expressing cyt.*c*-CFP were treated with TMRM and TNF-α. Delocalization of cyt.*c*-CFP and mitochondrial depolarization were observed with a resolution period of 1 min. All dying cells exhibited cyt.*c*-CFP release, mitochondrial depolarization, and shrinkage of the cell body. Figure 2A shows a typical fluorescent image of a dying cell. In this cell, cyt.*c*-CFP was released at 161 min, and cell shrinkage began at 167 min after the addition of TNF-α. Changes in TMRM fluorescence are plotted in Fig. 2B. TMRM fluorescence started to decrease at 164 min, thus indicating that the mitochondria started to depolarize at this point in time.

In a comparison of the starting points of these three events, it was found that the release of cyt.*c*-CFP always preceded mitochondrial depolarization and cellular shrinkage. Mitochondrial depolarization was observed earlier than cellular shrinkage in this particular cell, but was observed later in other cells. The temporal order of the timing of the initiation of mitochondrial depolarization and cellular shrinkage was not consistent. Mitochondrial depolarization preceded cellular shrinkage in 4 of the 10 cells, and cellular shrinkage preceded mitochondrial depolarization in 6 of the cells observed here.

Temporal relationships between mitochondrial changes, caspase activation, and cellular shrinkage

We observed 10 – 22 cells in each of these experiments, the results of which are shown in Figs. 1 and 2. We then determined the timing of cyt.*c* release, cellular shrinkage, and mitochondrial depolarization, or caspase activation in each cell. To clarify the temporal relationships between these cellular events, relative timing was

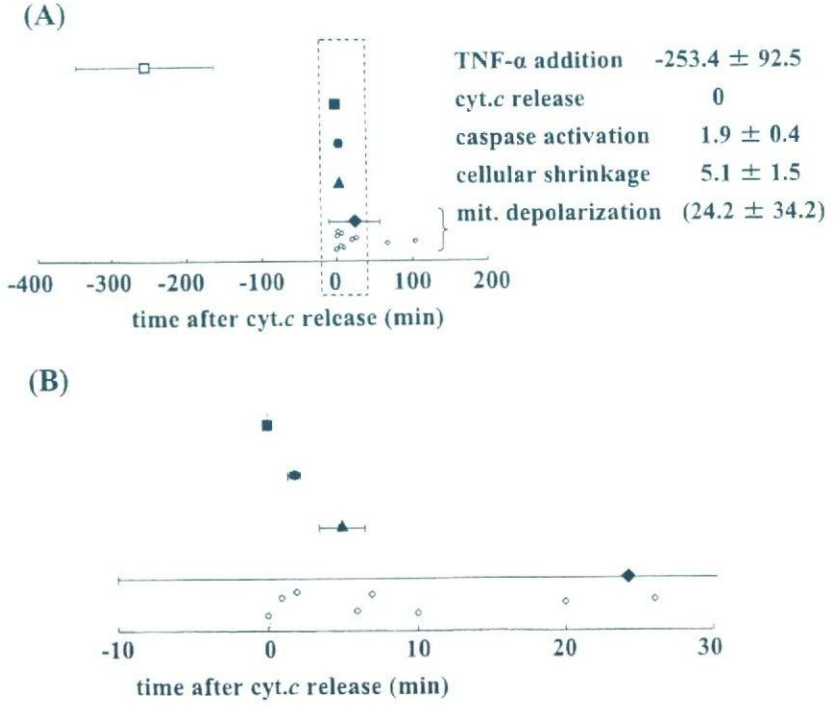

Fig. 3. Temporal relationship between mitochondrial changes and caspase activation. A: Relative timing of TNF-α addition (open square), cyt.*c* release (closed square), caspase activation (closed circle), cellular shrinkage (closed triangle), and mitochondrial depolarization (closed and open diamond) is shown with respect to time after cyt.*c* release. B: Shows a magnification of panel A.

determined as follows: the time point of cyt.*c* release was considered as time 0 in each of the individual cells. We calculated the relative timing of each of the observed events for each cell, and the results are plotted in Fig. 3. TNF-α treatment, cyt.*c* release, caspase activation, and cellular shrinkage are indicated as the mean ± S.D. Since mitochondrial depolarization did not give a normal distribution, all data for mitochondrial depolarization were plotted. Each plot represents the results from a single cell. Figure 3B shows magnification at around time 0.

The relative timing of TNF-α treatment and mitochondrial depolarization was found to deviate substantially, whereas the relative timing of caspase activation and cellular shrinkage gave only a small deviation. A substantial amount of time was required for the initiation of cyt.*c* release, and the duration varied between cells; however, after cyt.*c* release, the subsequent reactions occurred rapidly. After cyt.*c* release, cells are unable to stop or delay the cell death process.

Mitochondrial depolarization occurred before both caspase activation and cellular shrinkage in some of the cells (n = 4), but mitochondrial depolarization occurred after caspase activation and cellular shrinkage in other cells (n = 6). This finding suggests that mitochondrial depolarization is not necessary for either caspase activation or cellular shrinkage. Mitochondrial depolarization has been consistently reported as being associated with cell death, but it is not thought to be a critical step in the induction of apoptotic cell death.

Effects of the duration of TNF-α treatment

At the first step of TNF-α-induced cell death, TNF-α binds with its receptor on the cell surface, and an extracellular signal is transferred into the cell. After this step, Bid transfers the signal to the mitochondria, and then cyt.*c* is released from the mitochondria to the cytosol. Our results shown in Fig. 3 indicate that these processes took about 4 h. In order to analyze the timing of the onset of the earliest steps, we attempted to determine the point in time at which the first step started. To this end, we changed the duration of TNF-α exposure and measured the resulting cell survival rate. Cells were divided to two groups, as shown in Fig. 4A, and the cells were exposed to TNF-α for 0 – 12 h. In group A, the survival rate was measured immediately after TNF-α exposure. In group B, TNF-α was washed off after the indicated exposure time, and the cells were cultured in fresh medium without TNF-α for an additional 6 – 11 h, and the survival rate was then measured. If the cell death process proceeded after the removal of TNF-α, the survival rate would be expected to be reduced due to the additional culture period after the removal of TNF-α. In other words, more cells would be expected to have died in group B than in group A with the same amount of TNF-α exposure time.

The results showed that the survival rate decreased with increasing TNF-α exposure time (Fig. 4B). However, the survival rate did not decrease after TNF-α removal. This result suggests that the dead cells in group B had died during the period of TNF-α exposure, and that those cells that had survived during TNF-α exposure did not die after the removal of TNF-α. Thus, the cell death process is likely to proceed only when the cells were exposed to TNF-α. The survival rate in group B increased when cells were exposed TNF-α for 6 h. The biological meaning of this increase was unknown; however, this result did not disturb our conclusion.

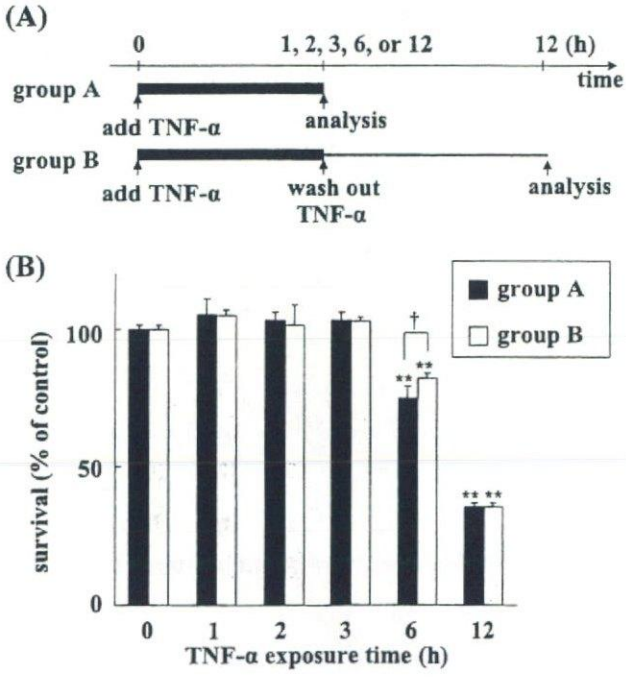

Fig. 4. Cell survival rate after TNF-α exposure. Panel A: Experimental design of the TNF-α exposure analysis. Thick lines represent the incubation in the presence of TNF-α, and thin line represents the incubation in the absence of TNF-α. In group A, cells were exposed to TNF-α for the indicated amount of time, and the cell survival rate was measured immediately. In group B, cells were exposed in the same manner as that used for group A. Then, the TNF-α was washed out, and the cells were cultured in fresh media for 6 – 11 h. Then, the cell survival rate was measured. The total duration of the culture period after the onset of TNF-α exposure was 12 h in group B. Panel B: The cells in groups A and B were exposed to TNF-α for 1, 2, 3, 6, or 12 h, and the cell survival rates were determined. Each bar represents a mean ± S.D. (n = 6). $^{**}P<0.01$ *vs* time 0, according to Dunnett's test. $^{\dagger}P<0.05$ between groups A and B, according to Student's *t*-test.

Discussion

This is the first report to reveal the precise temporal relationships between four reactions (mitochondrial depolarization, cyt.*c* release, caspase activation, and cellular shrinkage) in TNF-α-induced cell death. Because the onset of these reactions varied among individual cells, real-time single-cell imaging is the only currently available method to reveal temporal relationships between these reactions. We described our three-color real-time imaging technique in this report. Rehm et al. has reported the simultaneous real-time imaging of caspase activation and Smac release by using CFP/YFP-FRET sensor and YFP-tagged protein (26). They used the same color, YFP, for the observation of both reactions. It is possible to identify two reactions as they discussed, but it may be difficult to identify small changes occurring in the cell by their method. Previously, we revealed that DsRed was useful for FRET analysis of caspase activation (24). In this report, we observed caspase activation and cyt.*c* release with YFP/DsRed-FRET sensor and CFP-tagged protein. By using fluorescent probes in different colors, each reaction could be easily and precisely identified in a single cell.

We observed cell death at the single-cell level with a resolution period of 0.5 – 1 min, and we revealed that the relative timing between cyt.*c* release, caspase activation, and cellular shrinkage remained constant in all of the dying cells observed; however, the timing of mitochondrial depolarization showed a large deviation (Fig. 3). After cyt.*c* release, apoptosome formation, caspase-9 activation, caspase-3 activation, and the cleavage of various substrates that lead to apoptotic cell death are initiated. Our results revealed that this series of reactions takes place within 10 min and that the time course of this process was identical among all of the dying HeLa cells.

Mitochondrial depolarization was observed in all dying cells, but we considered that mitochondrial depolarization was not the cause of cyt.*c* release, caspase activation, and cellular shrinkage. Mitochondrial depolarization was found to occur at any time after cyt.*c* release. Mitochondrial depolarization was observed after caspase activation and cellular shrinkage in 60% of the observed cells. These results exclude the possibility that mitochondrial depolarization is a cause of cyt.*c* release, caspase activation, and/or cellular shrinkage. This is consistent with previous findings that cell death occurred without mitochondrial depolarization. Li et al. have shown that caspases are activated independently of mitochondrial depolarization in TNF-α-induced cell death (27). Krohn et al. have shown that cyt.*c* release and caspase activation occurred in the absence of mitochondrial depolarization in cell death of hippocampal neurons (28). Several studies suggested that mitochondrial depolarization is a critical step for cell death (29), but our results support the idea that mitochondrial depolarization is not crucial to the cell death process.

Cyt.*c* release may be a key step in two independent series of events, that is, the cell death process and mitochondrial depolarization. We speculate that cells might try to maintain cellular homeostasis by keeping membrane potential after cyt.*c* release. While maintaining the membrane potential, the released cyt.*c* immediately initiated the cell death process in the cytosol, and thus caspase activation and cellular shrinkage always took place within a short period of time. The timing of mitochondrial depolarization did not appear to be relevant to this process.

A number of imaging analyses have demonstrated that each cell death event is a rapid process. Initiator- and effector-caspase activation both proceed rapidly (23, 24, 30 – 32). Cyt.*c* is also released rapidly in a single step (33 – 35). Likewise, Smac/DIABLO is released rapidly, although the duration of Smac/DIABLO release is greater than that of cyt.*c* (26). Several multi-event imaging studies have suggested that cell death events occur almost simultaneously. Initiator caspase activation/effector caspase activation, effector caspase activation/mitochondrial depolarization, cyt.*c*/smac, and effector caspase activation/smac release had been analyzed simultaneously at the single-cell level and were found to occur almost simultaneously (24, 26). These findings, taken together with our present results, suggest that the cell death cascade proceeds rapidly after mitochondrial changes take place.

Once cyt.*c* was released, the following reactions proceed in a rapid manner. However, it did take 253.4 ± 92.5 min from TNF-α treatment to cyt.*c* release, and this duration varied from cell to cell (Figs. 3 and 4). We observed some cells that had died within 1 h in imaging analysis, indicating that cells have the ability to induce cell death within 1 h, and suggesting that certain factors may delay signal transduction and the timing of cell death. The results shown in Fig. 4 indicate that these factors were active only when the cells were exposed to TNF-α. We considered two possible explanations for these findings. 1: Each TNF-α molecule changed the cell slightly, and the changes induced by one molecule were not sufficient to induce the cell death cascade on their own. However, many TNF-α molecules attacked the cell, and intracellular changes thus accumulated. When the accumulated changes exceeded the threshold level, the cell death cascade would be expected to have

proceeded rapidly. 2: TNF-α could induce intracellular changes by chance. According to this explanation, TNF-α molecules would bind with the TNF receptor, but only some of them would be able to induce intracellular change. If some TNF-α molecules successfully induce intracellular changes, then the cell death cascade would proceed rapidly. The more TNF-α molecules that are present around the cell, and/or the longer these TNF-α molecules attack the cell, the higher the probability of a successful attack, and it can be expected that more cells will die. According to both of these models, the cell death process would not proceed in the absence of TNF-α exposure; therefore, those cells that survived during TNF-α exposure would not be expected to die after the removal of TNF-α.

One of the Bcl-2 family proteins, Bid, was cleaved to tBid due to the cell death signal, and the tBid transferred the signal from the cytosol to the mitochondria (36). Exogenous treatment with tBid is known to induce cell death immediately (37), and thus reactions that delay signal transduction may occur at an earlier step than either Bid cleavage or mitochondrial changes.

As cell death reactions often occur in a rapid manner and because the timing of the onset of intracellular reactions varies among cells, precise temporal relationships between cellular events during cell death should be further analyzed at the single-cell level with high temporal resolution. Single-cell imaging analyses of early stages (e.g., receptor oligomerization and the recruitment of adaptor proteins) will help to elucidate the mechanism of the entire cell death process.

Acknowledgments

This study was supported in part by a Grant-in-Aid for Research on Health Sciences focusing on Drug Innovation from the Japan Health Science Foundation; a Grant-in-Aid for Research on Advanced Medical Technology from the Ministry of Health, Labour, and Welfare; and a grant (MF-16) from the Organization for Pharmaceutical Safety and Research.

References

1 Thornberry NA, Lazebnik Y. Caspases: enemies within. Science. 1998;281:1312–1316.
2 Stennicke HR, Salvesen GS. Properties of caspases. Biochim Biophys Acta. 1998;1387:17–31.
3 Boldin MP, Goncharov TM, Goltsev YV, Wallach D. Involvement of MACH, a novel MORT1/FADD-interacting protease, in Fas/APO-1- and TNF receptor-induced cell death. Cell. 1996; 85:803–815.
4 Muzio M, Chinnaiyan AM, Kischkell FC, O'Rourke K, Shevchenko A, Ni J, et al. FLICE, a novel FADD-homologous ICE/CED-3-like protease, is recruited to the CD95 (Fas/APO-1) death-inducing signal complex. Cell. 1996;85:817–827.
5 Medema JP, Scaffidi C, Kischkel FC, Shevchenko A, Mann M, Krammer PH, et al. FLICE is activated by association with the CD95 death-inducing signaling complex (DISC). EMBO J. 1997;16:2794–2804.
6 Martin DA, Siegel RM, Zheng L, Lenardo MJ. Membrane oligomerization and cleavage activates the caspase-8 (FLICE /MACHalpha1) death signal. J Biol Chem. 1998;273:4345–4349.
7 Srinivasula SM, Ahmad M, Fernandes-Alnemri T, Litwack G, Alnemri ES. Molecular ordering of the Fas-apoptotic pathway: The Fas/APO-1 protease Mch5 is a CrmA-inhibitable protease that activates multiple Ced-3/ICE-like cysteine proteases. Proc Natl Acad Sci U S A. 1996;93:14486–14491.
8 Orth K, O'Rourke K, Salvesen GS, Dixit VM. Molecular ordering of apoptotic mammalian CED-3/ICE-like proteases. J Biol Chem. 1996;271:20977–20980.
9 Tewari M, Quan LT, O'Rourke K, Desnoyers S, Zeng Z, Beidler DR, et al. Yama/CPP32 beta, a mammalian homolog of CED-3, is a CrmA-inhibitable protease that cleaves the death substrate poly(ADP-ribose) polymerase. Cell. 1995;81:801–809.
10 Green DR, Reed JC. Mitochondria and apoptosis. Science. 1998;281:1309–1312.
11 Martinou JC, Green DR. Breaking the mitochondrial barrier. Nat Rev Mol Cell Biol. 2001;2:63–67.
12 Saleh A, Srinivasula SM, Acharya S, Fishel R, Alnemri ES. Cytochrome c and dATP-mediated oligomerization of Apaf-1 is a prerequisite for procaspase-9 activation. J Biol Chem. 1999;274:17941–17945.
13 Shiozaki EN, Chai J, Shi Y. Oligomerization and activation of caspase-9, induced by Apaf-1 CARD. Proc Natl Acad Sci U S A. 2002;99:4197–4202.
14 Tyas L, Brophy VA, Pope A, Rivett AJ, Tavare JM. Rapid caspase-3 activation during apoptosis revealed using fluorescence-resonance energy transfer. EMBO reports. 2000;1:266–270.
15 Rehm M, Dussmann H, Janicke RU, Tavare JM, Kogel D, Prehn JHM. Single-cell fluorescence resonance energy transfer analysis demonstrates that caspase activation during apoptosis is a rapid process: role of caspase-3. J Biol Chem. 2002;277: 24506–24514.
16 Luo KQ, Yu VC, Pu Y, Chang DC. Application of the fluorescence resonance energy transfer method for studying the dynamics of caspase-3 activation during UV-induced apoptosis in living HeLa cells. Biochem Biophys Res Commun. 2001;283:1054–1060.
17 Morgan MJ, Thorburn A. Measurement of caspase activity in individual cells reveals differences in the kinetics of caspase activation between cells. Cell Death Differ. 2001;8:38–43.
18 Tsien RY, Miyawaki A. Seeing the machinery of live cells. Science. 1998;280:1954–1955.
19 Miyawaki A, Sawano A, Kogure T. Lighting up cells: labeling proteins with fluorophores. Nat Cell Biol. 2003;S1–S7.
20 Tsien RY, The green fluorescent protein. Annu Rev Biochem. 1998;67:509–544.
21 Erickson MG, Moon DL, Yue DT. DsRed as a potential FRET partner with CFP and GFP. Biophys J. 2003;85:599–611.
22 Karasawa S, Araki T, Nagai T, Mizuno H, Miyawaki A. Cyan-emitting and orange-emitting fluorescent proteins as a donor

/acceptor pair for fluorescence resonance energy transfer. Biochem J. 2004;381:307–312.
23 Kawai H, Suzuki T, Kobayashi T, Mizuguchi H, Hayakawa T, Kawanishi T. Simultaneous imaging of initiator / effector caspase activity and mitochondrial membrane potential during cell death in living HeLa cells. Biochim Biophys Acta. 2004;1693:101–110.
24 Kawai H, Suzuki T, Kobayashi T, Sakurai H, Ohata H, Honda K, et al. Simultaneous real-time detection of initiator- and effector-caspase activation by double fluorescence resonance energy transfer analysis. J Pharmacol Sci. 2005;97:361–368.
25 Scaduto RC Jr, Grotyohann LW. Measurement of mitochondrial membrane potential using fluorescent rhodamine derivatives. Biophys J. 1999;76:469–477.
26 Rehm M, Dussmann H, Prehn JHM. Real-time single cell analysis of Smac/DIABLO release during apoptosis. J Cell Biol. 2003;162:1031–1043.
27 Li X, Du L, Darzynkiewicz Z. During apoptosis of HL-60 and U-937 cells caspases are activated independently of dissipation of mitochondrial electrochemical potential. Exp Cell Res. 2000;257:290–297.
28 Krohn AJ, Wahlbrink T, Prehn JHM. Mitochondrial depolarization is not required for neuronal apoptosis. J Neurosci. 1999;19:7394–7404.
29 Heiskanen KM, Bhat MB, Wang H-W, Ma J, Nieminen A-L. Mitochondrial depolarization accompanies cytochrome c release during apoptosis in PC6 cells. J Biol Chem. 1999;274:5654–5658.
30 Ohnuki R, Nagasaki A, Kawasaki H, Baba T, Uyeda TQP, Taira K. Confirmation by FRET in individual living cells of the absence of significant amyloid β-mediated caspase 8 activation. Proc Natl Acad Sci U S A. 2002;99:14716–14721.
31 Takemoto K, Nagai T, Miyawaki A, Miura M. Spatio-temporal activation of caspase revealed by indicator that is insensitive to environmental effects. J Cell Biol. 2003;160:235–243.
32 Luo KQ, Yu VC, Pu Y, Chang DC. Measuring dynamics of caspase-8 activation in a single living HeLa cell during TNFalpha-induced apoptosis. Biochem Biophys Res Commun. 2003;304:217–222.
33 Lim MLR, Lum M-G, Hansen TM, Roucou X, Nagley P. On the release of cytochrome c from mitochondria during cell death signaling. J Biomed Sci. 2002;9:488–506.
34 Goldstein JC, Waterhouse NJ, Juin P, Evan GI, Green DR. The coordinate release of cytochrome c during apoptosis is rapid, complete and kinetically invariant. Nat Cell Biol. 2000;2:156–162.
35 Goldstein JC, Munoz-Pinedo C, Ricci J-E, Adams SR, Kelekar A, Schuler M, et al. Cytochrome c is released in a single step during apoptosis. Cell Death Differ. 2005;12:453–462.
36 Luo X, Budihardjo I, Zou H, Slaughter C, Wang X. Bid, a Bcl-2 interacting protein, mediates cytochrome c release from mitochondria in response to activation of cell surface death receptors. Cell. 1998;94:481–490.
37 Madesh M, Antonsson B, Srinivasula SM, Alnemri ES, Hajnóczky G. Rapid kinetics of tbid-induced cytochrome c and Smac/DIABLO release and mitochondrial depolarization. J Biol Chem. 2002;277:5651–5659.